INCORPORATING REMOTELY-SENSED ROLLER PROPERTIES INTO SET-UP ESTIMATIONS FOR RANDOM WAVE CONDITIONS

Raúl P. Flores[1], Patricio A. Catalán[2] and Merrick C. Haller[3]

Abstract

High-resolution remote sensing video signals from surf zone waves in a large laboratory flume are analyzed with the purpose of directly measuring breaking wave quantities. The analysis is performed on a wave-by-wave basis using an image-processing algorithm to extract the cross-wave length of the wave roller from the optical intensity signal. The measured roller lengths are used to estimate roller dissipation, roller energy and roller contribution to the radiation stresses, which in turn are used to drive the mean cross-shore energy and momentum equations to obtain wave heights and mean water levels. The resulting profiles are compared against measurements from in-situ wave gages. Good agreement in predicting both parameters is achieved, thus providing a new approach to estimate breaking wave dissipation and roller forcing terms from remote sensing data. Since the methodology relies on estimation of a geometrical property such as the roller wave length, it can be applied with several remote sensors.

Key words: Remote sensing, breaking waves, energy dissipation, mean water level, wave roller, surf zone.

1. Introduction

An accurate description of nearshore hydrodynamics requires at least a good estimation of quantities such as wave heights, mean water levels and the forcing induced by wave breaking. In situ observations, numerical modeling or a combination of both methods can be used to obtain these quantities. The former are considered more accurate but are usually costly, and lack spatial resolution. Numerical wave transformation models used to predict nearshore hydrodynamics range in complexity, computational efficiency and accuracy. In order to capture the dynamics of wave breaking, most models require incorporating this process explicitly. For instance, wave transformation models based on the wave energy flux balance, typically introduce breaking wave parameterizations (Battjes and Jansen, 1978; Thornton and Guza, 1983). One common aspect of these parametric models is that they succeed in modeling wave height evolution but to improve estimation of other quantities such as set-up, the contribution of the breaking wave roller (the turbulent body of air and water carried onshore by the wave front) to energy and momentum balances cannot be neglected (Svendsen, 1984a,b). One of the main benefits of including these extra terms has been an improved modeling of the transition zone that exists immediately after breaking. Although wave height decay begins at the breakpoint, observations show that set-up initiates well beyond this point (Svendsen et al., 1978). The inclusion of the roller in the wave forcing causes a spatial lag between organized wave energy dissipation and the transfer of momentum to the water column, thus producing an onshore shift of maximum currents and set-up relative to breaking point (Nairn et al., 1990). Several roller evolution models have been developed (e.g. Lippmann et al., 1996, Dally and Brown, 1995; Stive and de Vriend, 1994). To estimate the spatial evolution of quantities such as wave height and mean water levels, a forward approach is used on which offshore waves are allowed to evolve as they progress over known. These models are typically calibrated with measured wave height profiles.

Regarding measurements, remote sensing tools have progressed significantly and have been used for quantitative coastal studies. Their synoptic nature allows capturing the high spatial and temporal variability of several nearshore processes. Furthermore, wave breaking signatures are usually very prominent in a number

[1]Departamento de Obras Civiles, Universidad Técnica Federico Santa María, Valparaíso, Chile. raul.flores@usm.cl
[2]Departamento de Obras Civiles, Universidad Técnica Federico Santa María, Valparaíso, Chile. patricio.catalan@usm.cl
[3]School of Civil and Construction Engr., Oregon State University, Corvallis, OR, USA. hallerm@engr.orst.edu

of different remote sensing techniques, such as optical or microwave systems, thus opening the possibility of directly measuring breaking wave quantities. For example, one aspect of the usage of optical systems in coastal monitoring is by linking high values of signal intensity with breaking wave dissipation. However, the relation is not straightforward since other phenomena (such as persistent foam in optical or steepened waves in microwave systems) still can contaminate the signal resulting in difficulties in the accurate discrimination of active breaking (the wave roller), which is the area of primary dynamical interest. For optical sensing, the most common image product used to estimate surf zone dissipation has been the time exposure (map of temporal mean of the optical signal) where the contributions of the wave roller and remnant foam are not accounted for separately. Therefore, this approach has been fairly qualitative and mostly associated with the spatial extension of the surf zone and its variability, and linked to morphologic variability. Aarninkhof and Ruessink (2004) developed a procedure to isolate roller contributions from the mean intensity image by introducing a model for the decay of the intensity signal. However, from a hydrodynamic standpoint, shorter timescales can be relevant and the contribution of individual waves can be of interest. Haller and Catalán (2009) analyzed the optical intensity signal and its relationship with roller geometrical characteristics for regular waves breaking over a barred bathymetry. They found that the optical signal of the wave roller ramps up from the toe of the roller on the front face of the wave to a maximum intensity at the wave crest. As a result, they proposed a new method to extract the cross-wave length of the wave roller from optical intensity.

This type of data can be now integrated to nearshore modeling efforts to improve estimations, provided an adequate linkage between measured quantities and model physics exists. For breaking waves, Duncan (1981) reported results of waves breaking in equilibrium for deep water conditions and provided measurements of roller cross-sectional area, slope and length. More recently, Govender et al. (2002) provided measurements of roller geometries under spilling and plunging waves for a few laboratory conditions using video imagery. These geometrical roller properties (cross-sectional area, and its angle of inclination) have been related to the dissipation rate of breaking waves (Duncan, 1981; Deigaard and Fredsoe, 1989) and the above-trough mass flux responsible for undertow generation (Garcez Faria et al., 2000).
In this work we follow these ideas and we couple remotely sensed data to a wave-averaged roller model to estimate wave heights and mean water levels in the surfzone. We focus on obtaining from the remote data dissipation rates and roller radiation stresses, which are then used as input to drive the numerical model. This methodology represents a new technique to obtain quantitative wave data from the surfzone.
The paper is organized as follows: in section 2 a review of the cross-shore energy and momentum balances including roller effects are presented. Section 3 describes the experimental set-up and data sources. Data processing procedures and results for wave heights and set-up using the proposed data assimilation process are presented in section 4, and a discussion of these results follows in section 5. Finally, section 6 presents conclusions and future work perspectives.

2. Theory

One approach to model nearshore hydrodynamics is to estimate the balance of wave-integrated flow properties, thus removing the need for an accurate description of small scale processes such as turbulence. Despite its overall simplicity, this approach is well suited for estimation of statistical properties such as wave height profiles and mean levels, at low computational costs. Here, a set of two coupled differential equations describing the time-averaged roller energy and cross-shore momentum balances is used to derive wave heights and mean water levels.

2.1 Roller energy balance

In the surf zone, the main source for the dissipation of organized wave energy arises from the interaction between the wave itself and the wave roller, mainly through the work done by the wave to feed and maintain the roller riding over its front face and travelling at its phase speed. The balance of organized wave energy can be written as (Battjes and Janssen, 1973)

$$D_{br} = -\frac{\partial}{\partial x}\left(E_w c_g\right) \tag{1}$$

where D_{br} is the wave dissipation, c_g is the group speed and E_w is the organized wave energy, taken from linear theory,

$$E_w = \frac{1}{8}\rho g H_{rms}^2 \tag{2}$$

in which ρ is the water density, g is the gravitational acceleration and H_{rms} is the root-mean-square wave height. Several models for the estimation of wave dissipation, D_{br}, are available in the literature (e.g. Battjes and Janssen, 1978; Thornton and Guza, 1983; Alsina and Baldock, 2007), and traditionally this equation is solved for H_{rms}.
Similarly, a roller energy balance equation can be obtained (Stive and De Vriend, 1994)

$$\frac{\partial}{\partial x}(2E_r c) = D_{br} - D_r \tag{3}$$

where E_r is the roller energy, c is the carrier wave phase speed, D_r is the roller dissipation. Roller energy can be estimated as (Svendsen ,1984a,b)

$$E_r = \frac{\rho A c}{2T} \tag{4}$$

where ρ is the average density of the roller (here assumed constant and equal to sea water density), A is the cross-sectional area of the roller and T is the wave period. In deriving this expression, it was assumed that the average velocity in the roller equals the wave celerity.
Roller dissipation is taken as the work done by the shear stress acting on the interface with the underlying wave. Considering that this shear stress must balance the weight of the roller in order for a force balance to exist (Duncan, 1981), the time-averaged rate of energy dissipation per unit platform area into the direction of roller motion reads (Dally and Brown, 1995)

$$D_r = \frac{\rho g A \sin\theta \cos\theta}{T} = \frac{2gE_r}{c}\sin\theta\cos\theta \tag{5}$$

where θ is the angle of inclination of the roller, which controls the amount of wave energy storage in the roller and its size. This parameter is not known a priori, but can be considered a free parameter to calibrate the model to achieve good reproduction of measured data.
Substituting Eqs. (1) and (5) into (3) and rearranging yields

$$\frac{\partial}{\partial x}\left(E_w c_g\right) = -\frac{\partial}{\partial x}(2E_r c) - \frac{2gE_r}{c}\sin\theta\cos\theta \tag{6}$$

where it can be seen that in solving for the energy flux (and hence wave height), it is required to know the roller parameters which depend on its geometry (A), and quantities that can be obtained from linear wave theory, if the bathymetry is known. We follow Duncan's (1981) experimental conclusion that the ratio of breaking region thickness, A/L (where L is the roller along-slope length), to length is constants for all observed conditions

$$\frac{A}{L^2} = 0.11 \pm 0.01 \tag{7}$$

This suggests that roller geometry is self-similar through most of its life cycle. To obtain L, we relate the horizontal projection of the roller, L_r , a remote sensing observable, to roller cross-sectional areas using $A = 0.11(L_r/\cos\theta)^2$. As a result of this, the only free parameter in Eq. (6) is the local surface slope θ, which is often taken as a calibration parameter in wave roller transformation models. Although we recognize that θ varies in time and space, here we consider this parameter as time-independent and cross-shore constant,

which has been the traditional approach (Dally and Brown, 1995; Apotsos et al., 2007). Typically, θ is assumed to be ~6º (Dally and Brown, 1995; Reniers and Battjes, 1997) although lower values have been reported (Walstra et al., 1996). We note that these values have been calibrated based on achieving the best adjustment to measured undertow and currents and not from direct roller data. In one of the few actual observations, Duncan (1981) reported a range of 10.0º< θ<14.7º, with a mean of 12.6º. Haller and Catalan (2009) implemented the procedure outlined above for monochromatic wave fields, obtaining good agreement with experimental H_{rms} profiles, with θ ~12.6 - 20º. The higher slope required suggests a slight underestimation of roller dissipation.

2.2 Cross-shore Momentum balance

The roller also affects the overall forcing in the nearshore through its contribution to radiation stresses. Assuming alongshore uniform bathymetry and negligible wind stress, the cross-shore momentum balance establishes that the net horizontal hydrostatic force due to wave set-up $\bar{\eta}$, balances the cross-shore gradient of the wave radiation stress, S_{xx}, and the bottom stress, τ_b (Longuet-Higgins and Stewart,1964)

$$\frac{\partial}{\partial x}S_{xx} + \rho g(\bar{\eta} + h)\frac{\partial}{\partial x}\bar{\eta} + \tau_b = 0 \tag{8}$$

where x is the cross-shore coordinate, h is the water depth, ρ is the water density and g is the gravitational acceleration. The cross-shore momentum balance can be considered to be dominated by radiation stress and set-up gradients, as supported by laboratory studies (Stive and Wind, 1982; Dally and Brown, 1995). Therefore, the effects of bottom stress are not considered ($\tau_b \approx 0$).
In the presence of breaking waves the radiation stress should be extended with the additional momentum induced by wave rollers (Svendsen, 1984), so that S_{xx} becomes

$$S_{xx} = S_{xx,w} + S_{xx,r} \tag{9}$$

where the first term on the right side represents the radiation stress associated with the organized wave motion, and the second term exists due to the presence of wave rollers. The wave component of the radiation stress is given by (Longuet-Higgins and Stewart, 1964)

$$S_{xx,w} = E_w\left(2\frac{c_g}{c} - \frac{1}{2}\right) \tag{10}$$

In turn, the contribution of the wave roller can be expressed as function of roller energy (Svendsen, 1984)

$$S_{xx,r} = 2E_r \tag{11}$$

Substituting Eqs. (10) and (11) into (8) and rearranging yields

$$\rho g(\bar{\eta} + h)\frac{\partial \bar{\eta}}{\partial x} = -\frac{\partial}{\partial x}\left[E_w\left(\frac{c_g}{c} - \frac{1}{2}\right)\right] - \frac{\partial}{\partial x}(2E_r) \tag{12}$$

Therefore, Eq. (12) allows estimation of the wave set-up when coupled with Eq. (6) by using as input roller data and the wave height profile, or in other words, to use the video derived data to obtain roller forcing in the nearshore.

3. Experimental Data

The experimental data were collected in the Large Wave Flume (LWF) at the O.H. Hinsdale Wave Research Laboratory (Oregon State University). The flume is approximately 90 m long, 3.7 m wide and 4.6 m deep. The x-axis is pointing onshore along the centerline of the flume, with origin at the wavemaker. The wavemaker is of the flap-type and is located at one end, where water depth was 4.27 m. The bathymetric profile was constructed using piecewise concrete slabs mounted on the tank walls and designed to

approximate the bar geometry of an observed field beach at a 1:3 reduction scale (Fig. 1).

Free surface elevation measurements were taken using six resistance-type wave gages sampling at 50 Hz. The wave gages were installed on the east wall at cross-shore locations x=23.45, 45.40, 52.73, 60.04, 70.99 and 81.97 m. as shown in Fig. 1. Sensors were located at specific positions: one offshore sensor to initiate wave models, three sensors over the bar region where breaking is expected, and two sensors located further onshore over the milder slope to characterize wave evolution as it approaches the shoreline. Wave runs were generated using narrow banded TMA spectrums (Bouws et al., 1985) with duration of 15 minutes. Four random wave conditions were tested and are listed in Table 1, and the corresponding H_{rms} wave heights are shown in Fig. 1. Iribarren numbers, $\xi = \beta/\sqrt{H_0/L_0}$ were computed using a representative slope $\beta = 1/24$, corresponding to the shoreward face of the bar, which is where breaking started for all conditions. The Iribarren numbers indicate that the breaking regime was spilling for all cases, which turns to be the most suitable type of breaker if using roller formulations. Further details of the experimental procedure can be found in Catalán and Haller (2008).

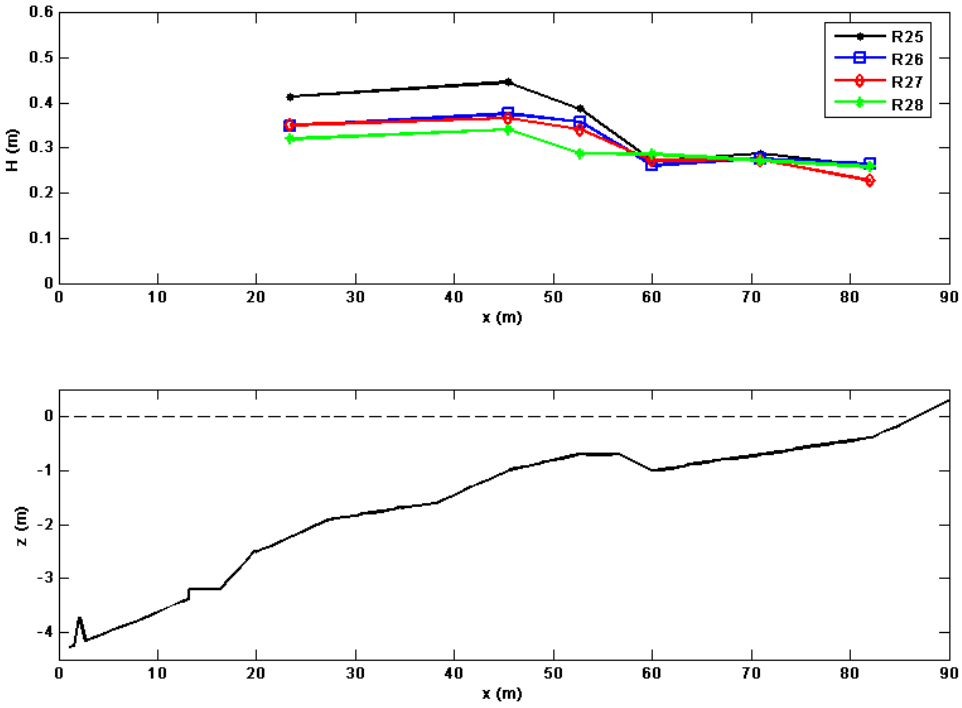

Figure 1. Experimental conditions: (top) measured wave heights for R25 (black), R26 (blue), R27 (red) and R28 (green) and (bottom) vertical elevation of the fixed bed.

Table 1. Wave conditions: Wave period T, deep water wave height $\boldsymbol{H_0}$, deep water steepness $\boldsymbol{H_0/L_0}$, Iribarren number $\boldsymbol{\xi_b}$ and Ursell number $\boldsymbol{Ur}$

Run	T (s)	$\boldsymbol{H_0}$ (m)	$\boldsymbol{H_0/L_0}$	$\boldsymbol{\xi_b}$	$\boldsymbol{Ur}$	Breaker Type
25	4	0.43	0.017	0.32	10.7	Spilling
26	5	0.34	0.009	0.45	15	Spilling
27	2,7	0.37	0.033	0.23	3.1	Spilling
28	4	0.29	0.012	0.39	7.7	Spilling

Simultaneous high-resolution video observations were captured using an ARGUS III video station (Holman and Stanley, 2007). At the time of the experiments the station consisted of three digital cameras mounted 9.88 m above still water level aimed at different sections of the flume, with a total field of view of the cameras spanning from x=41.7 m to the dry beach, capturing the complete extension of the surfzone. All cameras sampled at 10 Hz and were synchronized with the wave gages. For the analysis of the optical intensity data a cross-shore pixel array along the longshore coordinate y=1.2 m was used because it was the least perturbed by ambient lighting conditions. Actual camera resolution varies from 1 cm^2/pixel close to the cameras to 8 cm^2/pixel near the shoreline. The original rectified array (mapped to the elevation of the still water level) was interpolated to a uniform grid, with a total of 5736 pixels along the array with a resolution of Δx = 1 cm that preserved raw camera resolution. Further details of the video data processing can be found in Catalán (2005).

4. Data Processing and Results

The time series of optical intensity data from the cross-shore pixel array are arranged into a time-space map of pixel intensity, or "time stack" (Fig 2). Pixel intensity variations depend on the mechanism by which the waves are imaged by the camera. For unbroken waves, this mechanism is mainly specular reflection of the incident light on water surface, which is function of the instantaneous angle defined by the camera, the light source and the water surface; and also the relative angle between the direction of wave propagation and the camera. On the other hand, for breaking waves the main imaging mechanism is isotropic scattering from the aereated roller, comprised of droplets and bubbles, having a negligible dependency on system geometry.

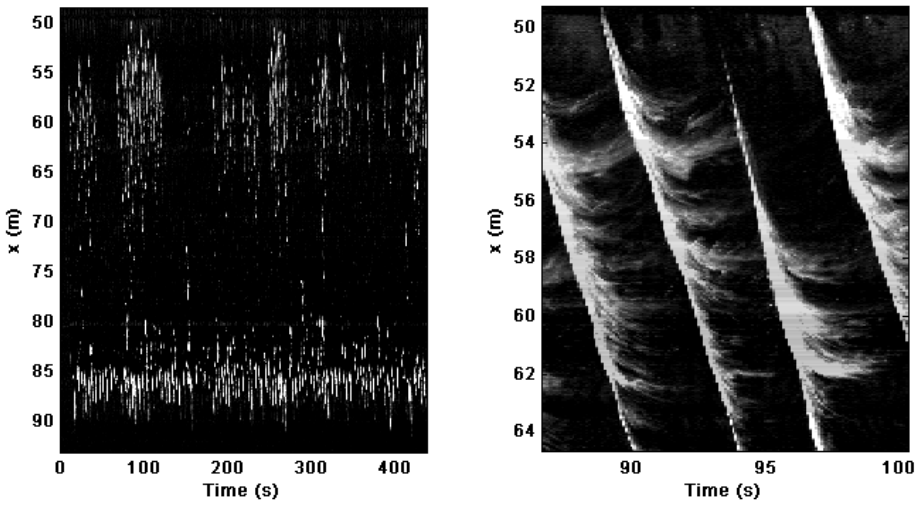

Figure 2. Example of timestack for Run 25 (left) Complete timestack where wave groups can be observed (right) Timestack close-up, with white regions correspond to breaking waves and foam. x=0 is at the wavemaker and the still water shoreline at x= 86 m.

4.1 Determination of roller lengths

Estimation of wave roller lengths from the data sets is performed on a wave-by-wave basis. First, isolation of breaking events is achieved by using an intensity threshold method, where all pixels with optical intensities above a threshold value are attributed to regions of wave breaking. The underlying assumption is that no breaking occurs without an optical signature. Following Haller and Catalán (2009), the intensity threshold here is chosen as $\bar{I} + 2\sigma_I$, where $\bar{I}$, σ_I are the mean and the standard deviation of the pixel intensity of a given timestack $I(x,t)$. Defined this way, the roller front edge corresponds closely to the zero crossing of the water surface signal. In Fig. 3 a pixel intensity spatial profile corresponding to a single timestep is shown. Wave fronts are characterized by a strong increase in pixel intensity, resulting in small sensitivity to the exact value of the intensity threshold chosen to identify individual events. The original timestack is then transformed into

a binary map of breaking and non-breaking waves, where a breaking event should be understood as grouping of connected pixels that exceed the selected threshold. We note that this breaking event selection does not account only for active breaking, but in fact large areas of remnant foam are detected. But since the method presented herein relies primary in the accurate identification of wave fronts, this represents no drawback.
Next, identification of wave fronts is performed using a tracking technique applied to the roller front as the breaking waves propagates toward the shoreline. For each instant, the roller leading edge is defined as the first pixel (from the shore) that exceeds the threshold intensity value. The trailing edge of the wave roller is defined as the point where intensity begins to decrease in the offshore direction. As a result, in Fig. 3 three breaking waves are identified. It is noticeable that some intensity values are clipped at 255 as a result of saturation of the cameras. This could have some effect in the determination of wave roller lengths due to the loss of information on the beginning of the intensity decay. However, pixel saturation was less than 1.5% for all wave runs analyzed here and possible errors in roller length estimation are expected to be minimum.

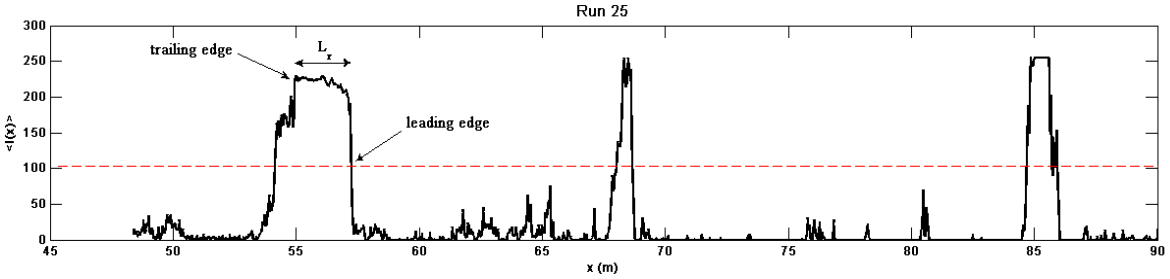

Figure 3. Example of optical intensity I(x) spatial profile for Run 25 at t=100 s. Red dashed line represents the threshold value used to identify wave fronts.

Applied to the entire timestack the methodology gives a time-space map of instantaneous roller lengths, as shown in Fig. 4 (upper panel). Consequently, for each spatial coordinate where breaking exists a root-mean-square roller length is determined, given by

$$L_{rms}(x) = \sqrt{\frac{1}{N_b(x)}\sum_{i=1}^{n} L_i(x)^2} \tag{11}$$

where $L_i(x)$ and $N_b(x)$ are the instantaneous roller lengths and the number of breaking waves associated with coordinate $X = x$. The reason for choosing root-mean-square roller lengths is consistency with parametric models solving the root-mean-square wave height. (e.g. Battjes and Janssen, 1978; Thornton and Guza, 1983) This assumes that the energy dissipation of an individual wave is adequately represented by a characteristic roller length. In this sense, L_{rms} is a representative parameter of the local dissipation at each section. Therefore, the model presented here is an alternative to models using the fraction of breaking waves to estimate breaking wave dissipation in the surf zone.

4.2 Estimation of Wave Height and Set-up from measured roller lengths

The process is then fairly straightforward. As we have mentioned before, this approach is different in the sense that we take advantage of new data to improve model estimations. First, we use remotely-sensed roller lengths to obtain direct estimations of roller dissipation, roller energy and roller contribution to radiation stress. Next, these quantities are incorporated into the cross-shore energy balance equation (Eq. 6) using a finite difference scheme which follows closely the procedure of Dally and Brown (1995) to calculate H_{rms} wave height. Finally, H_{rms} *(x)* gives an estimate of $S_{xx,w}$ which is used along $S_{xx,r}$ to yield the mean water

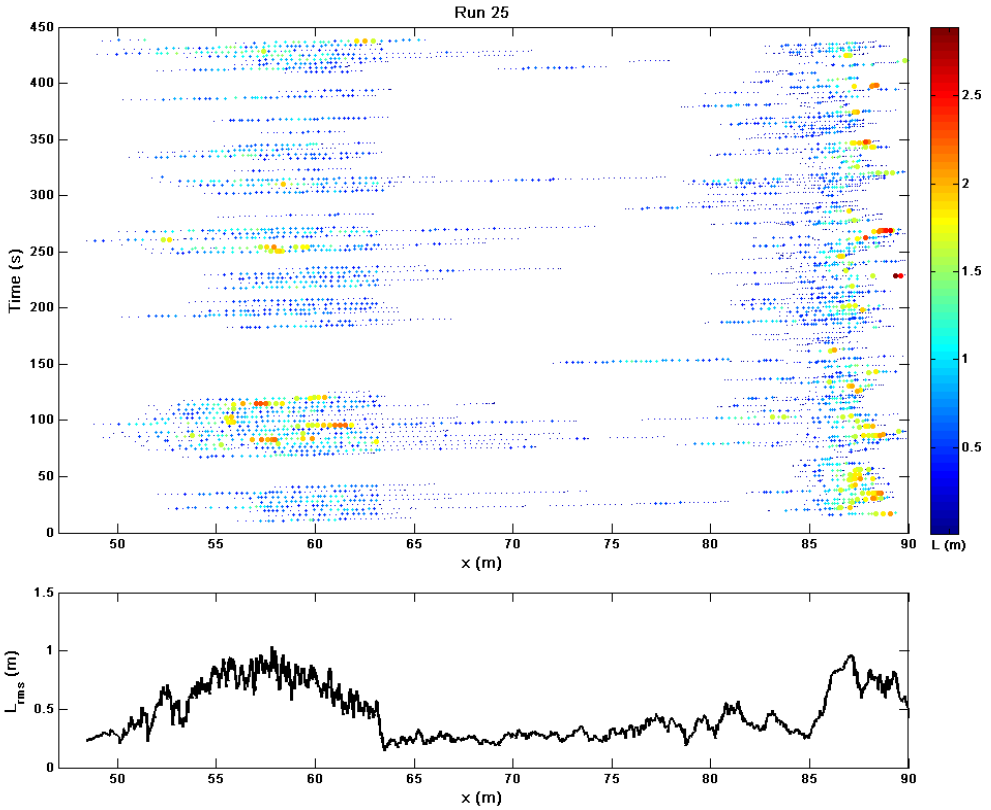

Figure 4. (Top) Time-space map of instantaneous roller lengths. (Bottom) Root-mean-square distribution of roller lengths.

level $\bar{\eta}$ (Eq. 8). The still water depth and wave period are assumed to be known. As a first approximation, wave properties such as celerity are taken from linear wave theory. The model is initiated with offshore boundary conditions for the wave energy, E_w, and the set-up, $\bar{\eta}$, taken at the most seaward sensor (x=23.45 m).

To calibrate our results, we test a range of θ values and we look for the best agreement to measured H_{rms} wave height profile. Model-data comparisons are evaluated by calculating absolute rms errors, defined by

$$\epsilon_{abs} = \sqrt{\frac{1}{N}\sum_{i=1}^{N}(P_i - O_i)^2} \cdot 100 \tag{13}$$

where $P_i$is the model prediction, O_i is the observed quantity, and N is the number of observations (in this case one for each sensor).

5. Results and Discussion

Figure 5 and 6 show results of wave height and setup profiles for Runs 25 and 27. Both wave height transformation and the mean water level compare favorably with the in-situ measurements taken by the wave gages. Table 2 shows the corresponding rms error, lower than 4% for all cases considered. A more detailed inspection shows that models struggle over the bar region, near the onset of breaking. Of all cases, best results are found for Run 27 (Fig. 6), which is the more linear case according to their Ursell number (see Table 1).

We note that the integrated decay through the surf is well captured, as can be seen from wave height prediction at the most shoreward wave gage. Hence, the total amount of dissipation (i.e. integrating D_r over the breaking region) obtained from the remotely-sensed data captures precisely the total decay of incident energy flux.

Calibrated roller slopes θ show little variability and are consistent with values given in the literature (Reniers and Battjes, 1997; Apotsos et al., 1993), as can be seen in Table 2. This suggests that the remotely-sensed roller length scale is consistent and does not need to be compensated by unreal values of θ to reproduce the necessary amount of dissipation to fit measured values.

Table 2. Calibrated surface slope and absolute error for analyzed wave cases.

Run	$\boldsymbol{\theta}$ (º)	$\boldsymbol{\epsilon_{abs}}$ (%)
25	11.0	3.56
26	7.5	3.19
27	8.0	0.55
28	8.5	3.59

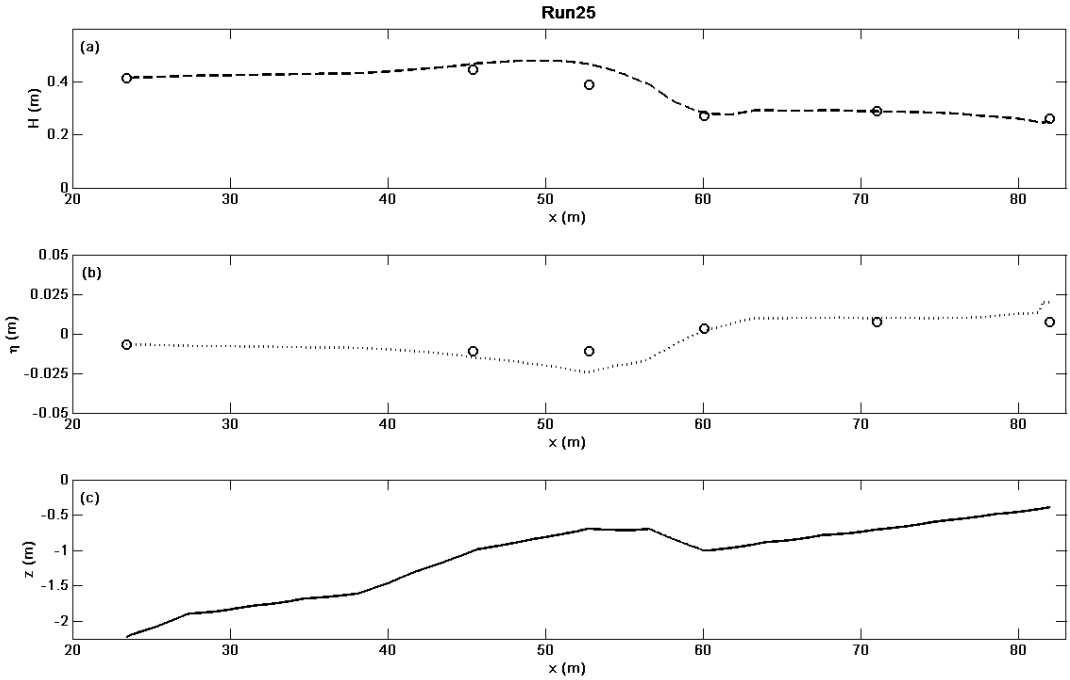

Figure 5. (a) Modeled $\boldsymbol{H_{rms}}$ profile (dashed line) and observed values (circles). (b) Modeled setup profile (dotted line) and observed values (circles) (c) Bathymetric profile.

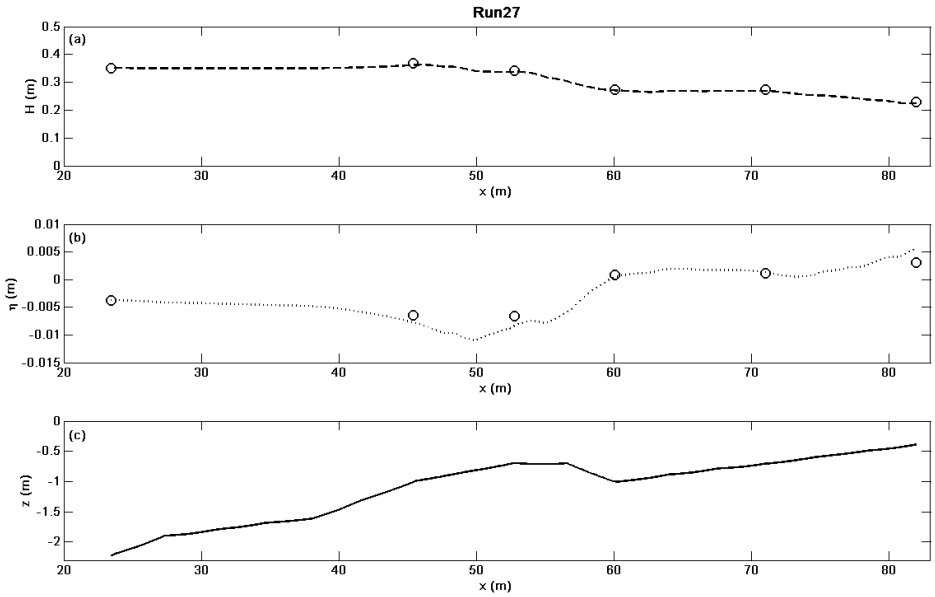

Figure 6. (a) Modeled $\boldsymbol{H_{rms}}$ profile (dashed line) and observed values (circles). (b) Modeled setup profile (dotted line) and observed values (circles) (c) Bathymetric profile.

Roller contribution to wave forcing can be seen in Figure 7, where wave roller and total radiation stresses are presented. The roller radiation stress increases when the wave begins to break, thus delaying the occurrence of a net onshore forcing and the development of wave set-up. Figure 7 also shows that roller contribution is significant, yet not the dominant component of nearshore forcing. However, at some cross-shore locations the contribution can be of the same order of magnitude of the wave component, particularly for Run 25, which is the most energetic of the conditions tested.

These results suggests that this methodological approach could be used to derive mean parameters such as wave heights and mean water levels when in situ data is scarce; or to compare against or validate model predictions. In order to assess the benefits of the methodology, results are compared with results of a roller model used in forward mode with standard parameters, θ=10º and γ=0.42 (Lippmann et al., 1996, henceforth LI96), the inverse roller model without including roller terms in the radiation stress and no set-up estimation (as in Haller and Catalan, 2009, HC09), and the proposed methodology including roller forcing. The inverse roller methods use an uncalibrated value of θ=10º for consistency in the comparison. We see an advantage in the sense that the inverse roller methods have only one free parameter to estimate (θ), which has a small variability range.

Figure 8 shows 3 cases: the LI96 wave model (dotted lines), HC09 approach (dashed lines) and the proposed approach (solid lines). It can be seen that the methodology proposed here shows better performance in reproducing both the wave height profile and the set-up profile, with little influence of including roller radiation stresses in wave height modeling since water depths are modified only slightly by set-up (dashed line and solid line converge in upper panel of Fig. 8). However, noticeable difference can be observed in the reproduction of the set-up profile, where the inclusion of roller radiation stresses gives overall best results, most notably in reproducing the spatial delay in set-up initiation. The use of a higher θ values than those determined during calibration leads to an overestimation of the dissipation, which upon integration through the surf zone, leads to an overestimation of set-up at the most onshore gage, for example in Run 27 (Fig 8, right panel).

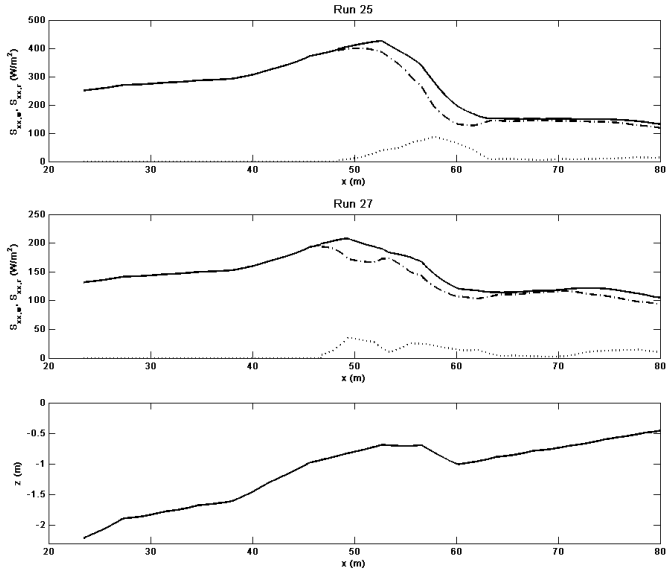

Figure 7. (top) Run 25: roller radiation stress (dotted line), wave radiation stress (dashed-dotted line) and total radiation stress (solid line) and (middle)) Run 25: roller radiation stress (dotted line), wave radiation stress (dashed-dotted line) and total radiation stress (solid line) and (bottom) bathymetry

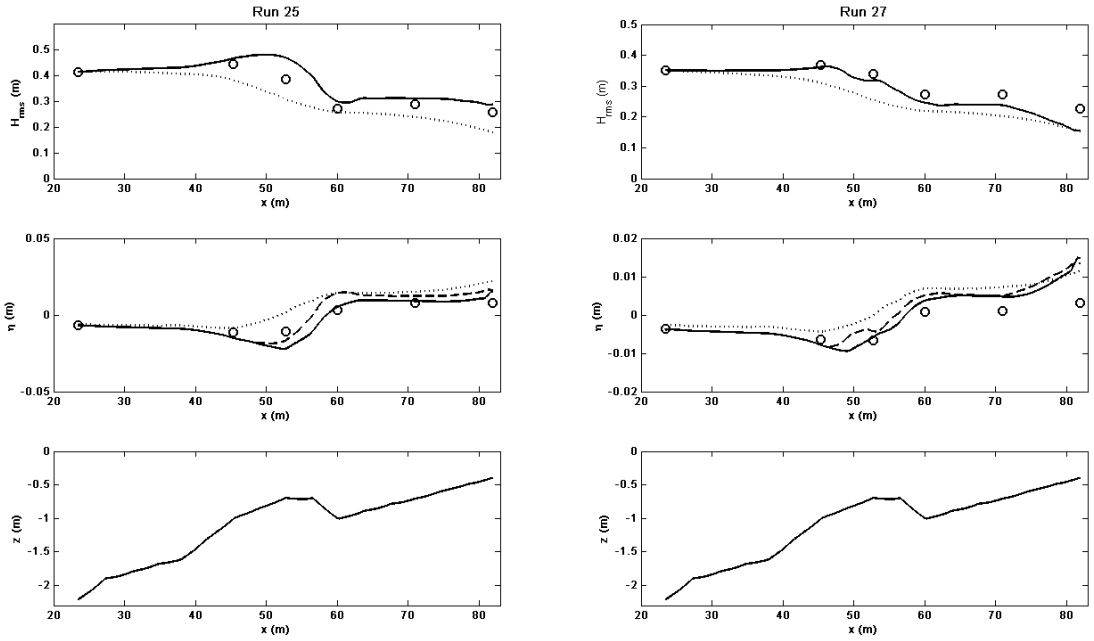

Figure 8. Sample estimation of wave parameters using a forward approach with standard parameters for the LI96 model (dotted lines), HC09 approach (dashed lines) and present approach (solid lines). (Upper panels) H_{rms} profile; (middle panels) set-up profile; (bottom panels) Bathymetry.

6. Conclusions

The objectives of the present study were to 1) analyze the optical signal from random wave fields over barred bathymetry to extract the cross-wave component of the wave roller length and 2) to develop a methodology to incorporate this remotely-sensed information into cross-shore energy and momentum balances to yield wave

height transformation and mean water levels. It was found that a video-derived root-mean-square roller length profile proved to be successful in the estimation of roller hydrodynamic properties for random wave fields, such as its energy, momentum flux and dissipation. Good agreement between measured and derived wave heights and set-up was found for all wave cases tested, suggesting a good physical link between the remotely sensed signal and surfzone processes. This link could be used for further nearshore modeling efforts, such as the estimation of roller mass flux and wave-driven currents. On the other hand, wave height and setup estimation are improved when compared to a standard model based on established calibration parameters (i.e. without calibration to this data set), providing a viable alternative when suitable data to perform model calibration are not available.

Future work involves testing and validating this new approach at field scales, and the examination of a potential full inversion model, since wave phase speed and bathymetry can also be derived from remotely sense data. On this regard, it is of note this approach can be used with other remote sensors as well, or a combination of them, the only requirement being the capability to extract roller geometry from the data.

Acknowledgements
This work was supported in part by FONDECYT through Grants 11090201 and 1120878. Special thanks to the folks at O.H. Hinsdale Wave Research Facility, and Rob Holman and the CIL group at Oregon State University.

References

Aarninkhof, S., and B. G. Ruessink, 2004, Video observations and model predictions of depth-induced dissipation, *IEEE Transactions on Geoscience and Remote Sensing, 42(11), 2612-2622*.

Alsina, J. M., and T. E. Baldock, 2007, Improved representation of breaking wave energy dissipation in parametric wave transformation models, *Coastal Eng., 54(10), 765-769*.

Apotsos, A., B. Raubenheimer, S. Elgar, R. T. Guza, and J. A. Smith, 2007, Effects of wave rollers and bottom stress on wave setup, *J. Geophys. Res., 112(C2), C02003*.

Battjes, J. A., and J. P. F. M. Janssen, 1978, Energy loss and set-up due to breaking in random waves, *Proc. Coastal Eng. Conf., 16, 569-587*.

Buows, E. H. Gunther, W. Rosenthal, and C. Vincent, 1985, Similarity of the wind wave spectrum in finite water depth, *J. Geophys, Res., 90(C1), 975-986*.

Catalán, P., 2005, Hybrid approach to estimating bathymetry using remote sensing, M. Oc. E. Thesis, Oregon State Univ.

Catalán, P. A., and M. C. Haller, 2008, Remote sensing of breaking wave phase speed with application to nonlinear depth inversion, *Coastal Eng., 55, 93-111*.

Dally, W. R., and C. A. Brown, 1995, A modeling investigation of the breaking wave roller with application to cross-shore currents, *J. Geophys. Res., 100(C12), 24873-24883*.

Deigaard, R., and J. Fredsoe, 1989, Shear stress distribution in dissipative water waves, *Coastal Eng., 13, 357-378*.

Duncan, J., 1981, An experimental investigation of breaking waves produced by a towed hydrofoil, *Proc. R. Soc. London, Ser. A, 377(1770), 331-348*.

Garcez Faria, A. F., E. B. Thornton, T C. Lippmann, and T. P. Stanton, 2000, Undertow over a barred beach, *J. Geophys. Res., 105(C7), 16999-17010*.

Govender, K., G. P. Mocke, and M. J. Alport, 2002, Video-imaged surf zone wave and roller structures and flow field, J. Geophys. Res., 107(C7), 3072.

Haller, M. C., P. A. Catalán, 2009, Remote sensing of wave roller lengths in the laboratory, *J. Geoph. Res, 114, C07022*.

Holman, R., and J. Stanley, 2007, The history and technical capabilities of Argus, *Coastal Eng., 54, 477-491*.

Longuet-Higgins, M. S., and R. W. Stewart, 1964, Radiation stress in water waves; a physical discussion with applications, *Deep Sea Research, 11, 529-562*.

Nairn, R. B., J. A. Roelvink, and H. N. Southgate, 1990, Transition zone width and implications for modeling surf zone hydrodynamics, *Proc. Coastal Eng. Conf., 22, 68-81*.

Reniers, A. J. H. M., and J. A. Battjes, 1997, A laboratory study of longshore currents over barred and non-barred beaches, *Coastal Eng., 30, 1-22*.

Stive, M. J. F., and H. G. Wind, 1982, A study of radiation stress and set-up in the nearshore region, *Coast. Eng., 6, 1-25*.

Stive, M. J. F., and H. J. de Vriend, 1994, Shear stresses and mean flow in shoaling and breaking waves, *Proc. Coastal Eng. Conf., 24,594-608.*

Svendsen, I.A., P.A. Madsen, J.B. Hansen, 1978, Wave characteristics in the surfzone, *Pro. Coast En. Conf, 16, 520-539.*

Svendsen, I. A., 1984a, Wave heights and set-up in a surf zone, *Coastal Eng., 8, 303-329*.

Svendsen, I. A., 1984b, Mass flux and undertow in a surf zone, *Coastal Eng., 8, 347-365*.

Thornton, E. B., and R.T. Guza, 1983, Transformation of wave height distribution, *J. Geophys. Res., 88(C10), 5925-5938.*

Walstra, d. J. R., G. P. Mocke, and F. Smit, Roller contributions as inferred from inverse modeling techniques, *Proc. Coastal Eng. Conf., 25, 1205-1218*.